Research Article | Vol. 8, No. 9 | 1 Sep 2018 | OPTICAL MATERIALS EXPRESS 2722
Optical Materials EXPRESS

Refractive index patterning of infrared glass ceramics through laser-induced vitrification [Invited]

MYUNGKOO KANG,[1,3,*] LAURA SISKEN,[1,3] JUSTIN COOK,[1] CESAR BLANCO,[1] MARTIN C. RICHARDSON,[1] ILYA MINGAREEV,[1,2] AND KATHLEEN RICHARDSON[1]

[1]*CREOL, College of Optics and Photonics, University of Central Florida, 4304 Scorpius St., Orlando, FL 32816, USA*
[2]*Department of Mechanical and Aerospace Engineering, Florida Institute of Technology, 150 W. University Blvd., Melbourne, FL 32901, USA*
[3]*M. Kang and L. Sisken contributed to this work equally.*
**myungkoo@creol.ucf.edu*

Abstract: Refractive index modification in glass or crystalline materials typically involves conversion of state (amorphous to crystalline or crystalline to amorphous) through a homogeneous, external stimulus such as laser- or current-induced heating, melting, or localized (resonant) bond modification. With the exception of traditional phase change materials that exploit reversibility, usually at high speeds and over multiple cycles, localized patterning of the refractive index is most frequently employed to induce a complete change of phase to enable the creation of embedded or surface optical structures. The present effort employs a novel, laser-induced vitrification (LIV) process developed to spatially modify the refractive index in a fully homogeneous glass ceramic material. Such processing leads to a local re-vitrification of the pre-existing nanocrystalline microstructure within the material to realize spatially-defined, refractive index profiles. Post-processing refractive index modification on the order of Δn ~-0.062 was realized in a partially crystallized, multi-component chalcogenide glass ceramic nanocomposite, subjected to bandgap laser exposure. Spatially-varied phase modification in the lateral and axial directions within a bulk glass ceramic is quantified and the optical function of the resulting structure is demonstrated in the formation of an infrared grating. The underlying mechanism associated with the resulting local refractive index modification is explained through quantification of the multi-phase material attributes including parent glass properties, crystal phase identity and phase fraction as determined through micro-XRD and electron microscopic analysis. This correlation validates the proposed mechanism associated with the modification. A threshold power density for LIV in the starting glass ceramic has been determined based on exposure conditions and material attributes.

1. Introduction

Infrared (IR) optical systems have increased in their applications across a wide range of commercial and defense platforms [1–4]. A primary driver in this thrust for such systems is a reduction in their size, weight, and power (SWaP), while improving or maintaining optical performance [5]. Traditional IR optical imaging systems typically employ bulk crystalline materials which can be costly to fabricate and form into optics. As there are a limited number of IR transparent crystals that can be manufactured into a desired size, shape and form, this gives limited material options to optical system designers to optimize system performance in new and more complex designs. These constraints may require the incorporation of additional optical elements to correct for various aberrations in such systems [5–7]. Among materials that can be used to improve material availability and to reduce fabrication cost for use in IR

#330083 https://doi.org/10.1364/OME.8.002722
Journal © 2018 Received 25 Apr 2018; accepted 30 Jul 2018; published 17 Aug 2018

Optical Materials EXPRESS

optics, chalcogenide glasses (ChGs) are becoming more widely used, due to their high transparency in the IR and the ability to modify their refractive index through compositional tailoring [1,4,8–17]. Recently, efforts to further tailor a glass' local index in a spatially varying way has been demonstrated through the partial crystallization of the glass, forming an optical nanocomposite [10,14,16] or more recently, through a micro-poling process [17]. In the former efforts, a glass ceramic is formed where the nanoscale crystallites are dispersed in the glassy phase, yielding an effective refractive index, n_{eff}, which differs from that of the parent starting material. In order to create varying amounts of crystallization within the ChG, laser irradiation is used to control either the formation of starting nuclei and/or their growth, in all three dimensions. Thus, this approach is now considered promising as a method to create useful ChG-based IR GRIN optics [10,14,16].

Meanwhile, as a result of some of the limitations related to the choice of laser conditions and the lack of repeatability of material modification in laser-induced crystallization [14], an alternative strategy has been sought to create a spatially varying amorphous/crystallized material that exhibits a transition in properties related to the transition between these two states. The spatial control of the extent of crystallization locally within the material with a laser beam is similar to prior developments with phase change materials (PCMs) [18–20]. PCMs exhibit a change from a glassy state to a fully crystalline state, and with certain materials, the reverse can also be induced creating multiple write/erase cycles. We propose the added potential through the use of multi-phase glass ceramics to have not only on and off states, extremes in the amorphous or fully crystallized state, but also to be able to reach any number of intermediate states allowing a finer control of the index variation in space within the material. Here, we present the findings of our investigation of an approach converse to the laser-assisted crystallization technique. This laser-induced vitrification (LIV) method starts with a glass ceramic and selectively re-amorphizes it through the controlled conversion of the crystalline phase(s) present. Specifically, the strategy involves starting with a glass ceramic and the creation of an index modification by locally reversing the extent of crystallization by melting of the previously established (nano-) crystals. Such modification is schematically depicted in Fig. 1. Here, the melting can be spatially controlled by a laser beam, and thus represents how the term laser-induced vitrification was coined [21]. The resulting re-amorphization creates a laser-modified region possessing a higher volume fraction of glassy phase with a lower index than the surrounding (starting) glass ceramic material, opposite to the previously reported index gradient imparted through the growth of the higher index crystalline phases within a starting (lower index) glass material [14,16,21].

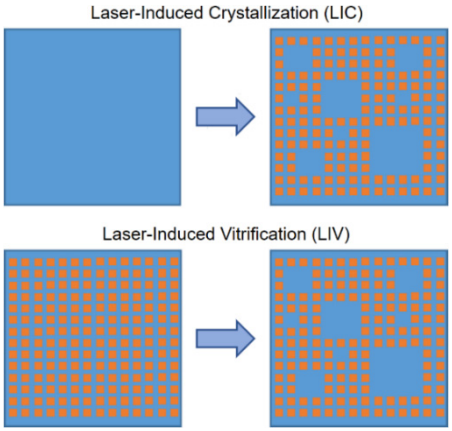

Fig. 1. Comparison of laser-assisted modification strategies used in this work. (TOP) Laser-induced crystallization (LIC), employs a homogeneous base glass material (blue) and then selectively grows crystals (red) in specific spatial locations. (BOTTOM) The reverse of this process, laser-induced vitrification (LIV), modifies a multi-phase glass-ceramic (red and blue

Optical Materials EXPRESS

represent crystal and glass phases), re-amorphizing local regions through spatially-selective laser exposure and vitrification.

2. Experimental

This study employs a multi-component $15GeSe_2$-$45As_2Se_3$-40PbSe (15-45-40 GAP-Se) glass material which has previously been investigated for gradient refractive index (GRIN) modification through use of a thermal gradient [14]. The parent glass material was prepared using traditional melt/quench protocols with 5N pure elemental starting materials in a 400 g batch [10]. This material was pre-crystallized to form a homogenous glass ceramic (GC) using a two-step furnace heat treatment (HT) with a nucleation step at 190 °C for 2 hrs followed by a growth step at 220 °C for 30 min. Important optical and material parameters of 15-45-40 GAP-Se parent glass and glass ceramic specimens from our previous studies are tabulated in Table 1 [10,21]. In this study, the parent glass (pre-HT) material was characterized with Raman spectroscopy to assess structure and Fourier-Transform infrared (FTIR) spectroscopy to measure infrared transmission. The post heat-treated glass ceramic material was characterized with FTIR spectroscopy, Raman spectroscopy, transmission electron microscopy (TEM) to assess crystal phase presence, and grazing-incidence micro *x*-ray diffraction (μ-XRD) to quantify crystalline and amorphous phases in the material. Transmission was measured using both a ThermoFisher Nicolet iS5 FTIR spectrometer and a CARY 500 UV-VIS spectrophotometer in order to cover the full spectral range of the material. Raman spectroscopy was measured using a Bruker Senterra system with an excitation wavelength of 785 nm, a power of 1 mW, a beam spot size of 2μm, a 20X objective, and a measurement time of 2.25 min at each location, ensuring that measurement conditions did not impart any surface/bulk modification. Raman mapping was carried out over an area of 16 μm × 16 μm by translating the sample under this exposure condition. For TEM studies, a cross-sectional specimen of a laser-exposed region with a width of 10 μm and a depth of 8 μm was prepared by ion milling followed by lift-out processing in a FEI 200TEM FIB. The sample was then mounted on a Cu grid and ion polished to ~50 nm in thickness to be electron transparent. TEM imaging and selected area electron diffraction (SAED) were carried out in a FEI Tecnai F30 TEM with an electron beam acceleration voltage of 80 kV. μ-XRD measurements were performed using a PANalytical Empyrean system with a beam wavelength of 0.15418 nm, a beam voltage of 45kV, a beam current of 40 mA, a beam spot diameter of 50 μm, and a grazing incidence angle of 5° at room temperature.

Table 1. Optical and material parameters of 15-45-40 GAP-Se parent glass and post-heat treated starting glass ceramic specimens

Specimen / Property	Parent glass	Glass ceramic
Refractive index (at λ = 4.5 μm and T = 22 °C)	3.04	3.14
Absorption coefficient (at λ = 1.030 μm)	8.22 cm^{-1}	50.40 cm^{-1}
Density (at T = 22 °C)	5.48 g/cm^3	5.43 g/cm^3
Glass transition temperature (heating rate 10 °C /min)	201 °C	
Crystallization temperature	259 °C	

Laser irradiation of the bulk chalcogenide glass ceramic substrate was performed using an Amplitude Satsuma fiber laser system with a wavelength of 1030 nm, a pulse duration of 350 fs, a repetition rate of 1 MHz, and an average power of 9.25 mW. Focusing was performed using a 5X/NA = 0.12 microscope objective, resulting in spot sizes of 4.43 μm. The sample was translated using an Aerotech ALS-130 3D positioning stage. A schematic of the laser/sample irradiation geometry and a plot of computed depth-dependent laser power density are shown in Fig. 2. Specifically, an irradiation protocol to realize pillar-like

Optical Materials EXPRESS

structures within the bulk (sub-surface) volume of the nanocomposite was developed whereby repeated translation of the irradiation volume in the z-direction followed by translation in the lateral direction (red arrows) allowed the glass ceramic's exposure with a high intensity focal volume of the laser possessing a beam waist of 4.43 μm, as shown in Fig. 2(a). Through this local treatment, pillars were created in the axial (z-direction) of the specimen at a position well below (mm's) the sample surface. Each individual pillar was nominally the width of the laser beam. Here, the irradiating beam is initially focused 1.87 mm below the substrate's surface and the substrate is subsequently translated 1.00 mm down in the z-direction, translating the focus of the laser towards the surface. As will be shown, this exposure protocol enabled a deeper amount of modified (amorphized) change and allowed easier characterization post-irradiation to demonstrate modification of the bulk material. As shown in Fig. 2(b), pillar structures processed by the above irradiation protocol were written in two-dimensional (2-D) line patterns to create a grating structure with a target width of ~9 μm and a spacing of ~60 μm to demonstrate optical functionality. Since the focal volume of the laser is located beneath the surface, it is expected that the modified focal region experiences a 'dose' of radiation that can be described by the competing effects of the target material's absorption-induced decrease in laser power density as a function of depth (commonly described by the Beer-Lambert law) and the buried laser's focal volume-induced increase in laser power density as a function of depth. Laser power density is quantified as a function of depth, using calculations based on a Zemax software macro where laser exposure condition and target material parameters specified in Table 1 were considered, as shown in Fig. 2(c). It is evident that the maximum laser power density increases as the depth approaches the position where the pillar is located. Importantly, the depth profile of the maximum laser power density within the region between the surface and the buried focal volume (i.e., pillars) implies a varying degree of LIV, and necessitates microstructural analyses to substantiate the type and magnitude of the modification which occurs within the range. These details will be discussed in the later part of this article.

Optical Materials EXPRESS

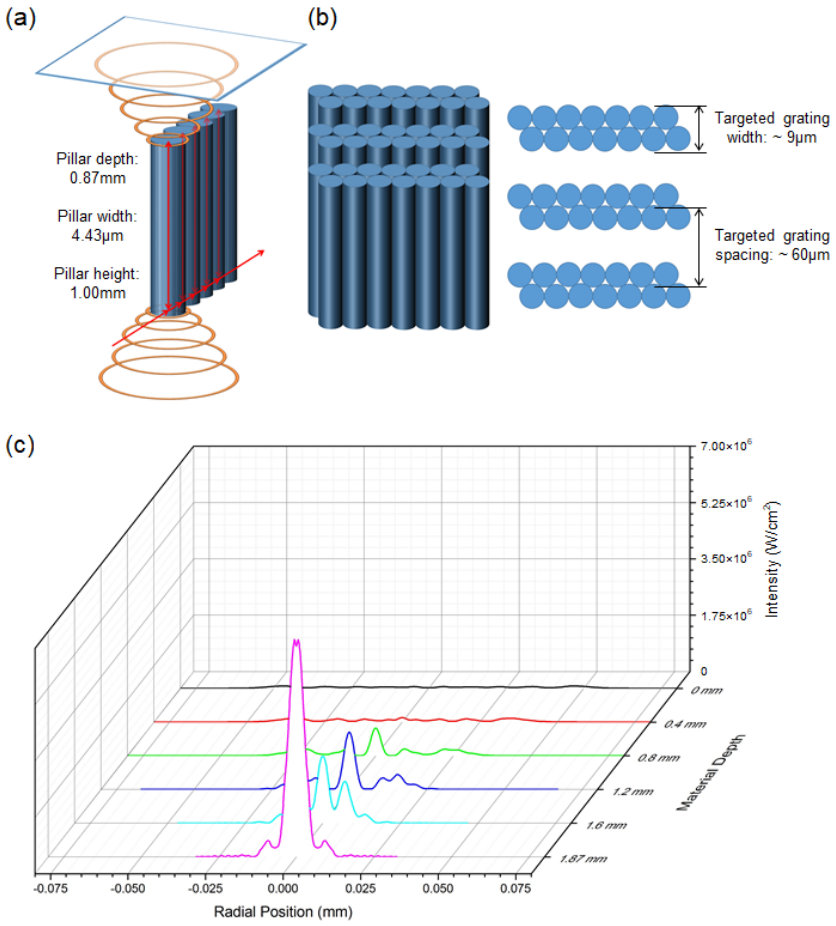

Fig. 2. (a) Laser irradiation geometry with its translational direction along red arrows and resulting pillars with a depth of 0.87 mm, a width of 4.43 μm, and a height of 1.00 mm. The concentric rings are meant to depict the varying focal area associated with the beam waist above and below the focal point. (b) Resulting grating structure with a targeted width of ~9 μm and a targeted spacing (period) of ~60 μm. (c) Computed depth-dependent laser power density as a function of radial position (irradiation area width at a fixed depth) as a function of depth below sample surface where pillar writing was started.

3. Result and discussion

The starting glass ceramic material was fully characterized prior to irradiation in order to provide a baseline for any measurable changes in properties that were observed following the irradiation. Figure 3(a) illustrates the transmission spectra of both the starting glass ceramic and parent glass materials. The glass ceramic transmission spectrum exhibits a slight scatter tail and a much higher absorption at the irradiation wavelength (λ = 1030 nm) as compared to the parent glass material. The laser wavelength used in this study is shown as the dotted vertical line on the transmission spectra, as shown in Fig. 3(a). This variation in transmission between glass and glass ceramic arises from the nanoscale Pb-containing crystallites present in the glass ceramic's matrix, as indicated by the asymmetric bright features in the dark field (DF) TEM image and the crystalline spots in the corresponding SAED pattern in Fig. 3(b). As the wavelength of the laser was in the highly absorbing region of the material's short wavelength optical band-edge, consideration of how best to ensure that the writing laser radiation penetrated the near surface region of the material without inducing ablation damage on the surface, is crucial. The variation in transmission between the glass ceramic and the

Optical Materials EXPRESS

glass indicates that transparency of the material increases as crystallization is reduced. A laser-vitrified region would then be expected to be more transparent to the irradiating beam, allowing penetration below the surface without ablation or damage. This modification allows laser penetration and amorphization to be achieved further into the sample during the irradiation process, rather than at the highly absorbing surface of the glass ceramic. Therefore, the vertical translation of laser focal point (through the 2 iterations of vertical movement in the pillar writing process) and the resulting pillars enable a larger amount of modified (amorphized) change and allows both easier characterization post-irradiation and further transparency to the writing beam to enable further modification of the bulk. The Raman signature of the glass ceramic material is also shown in Fig. 3(c). Raman spectroscopic characterization allows a clear delineation of structural variation between the parent glass and the post-HT'd glass ceramic. The Raman spectra of the glass ceramic exhibits two bands centered at wavenumbers of 205 cm^{-1} and 246 cm^{-1} where the peak located at a wavenumber of 205 cm^{-1} corresponds to Ge-Se bonds within $GeSe_2$ units, while the peak located at a wavenumber of 246 cm^{-1} consists of two major peaks located at wavelengths of 225 cm^{-1} and 240 cm^{-1} which can be attributed to As-Se vibrations found .within As_2Se_3. A shoulder located at a wavelength of 250 cm^{-1} originates from a peak corresponding to Se [14,21–23].

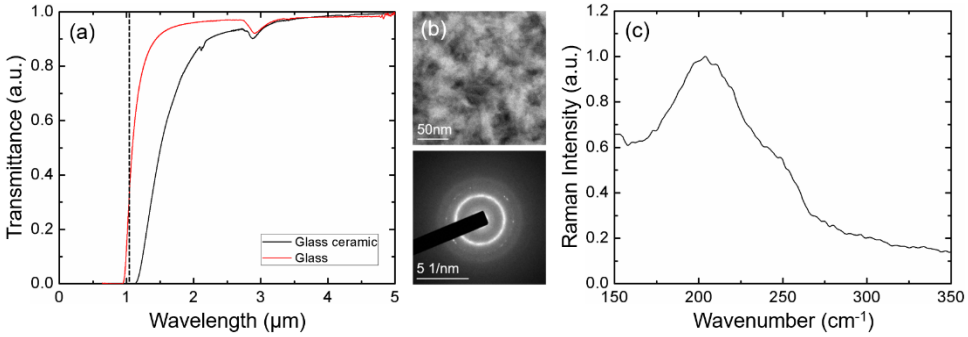

Fig. 3. (a) Transmittance spectra illustrating a variation in optical transmittance (sample thickness: 3 mm, corrected for Fresnel loss) between glass ceramic and glass materials. The dotted vertical line indicates laser wavelength. (b) A DF TEM image (top) and a corresponding SAED pattern of the starting glass ceramic material (bottom). (c) Raman spectrum of a glass ceramic material, measured using excitation wavelength of λ = 785 nm.

Raman spectroscopy was then used following irradiation to assess if the laser processing resulted in a modification to the post-processed material's Raman signature, whereby the partially amorphized starting glass ceramic exhibited structural changes moving back towards that of the parent base glass. Figure 4(a) shows the Raman spectra of both the starting glass ceramic and parent glass materials. Spectral differences in the Raman data between the glass ceramic material and the glass material exhibit a clear transition in bands representative of structural features within the respective materials. Here, the intensity of the peak at 246 cm^{-1} substantially increases in intensity while that of the peak at 205 cm^{-1} remains largely unchanged, indicating a clear change in the ratio of Ge-Se to As-Se bonds following conversion. The change in the ratio of these peaks is due to the conversion of As-Se bonds in the crystalline configuration (from crystalline As_2Se_3) to As-Se bonds in a more disordered, amorphous configuration. Characteristic bond configurations shown for the glass as compared to the partially amorphized glass ceramic (exhibiting a transition between the endpoints shown in Fig. 3a), would be clear indications of bond reorganization, consistent with bonding changes expected if nano-crystallites were melted and rapidly cooled to form disordered structural arrangement. One would also expect a localized change in density to occur upon reduction in the localized fraction of higher density crystallites, converting back to a lower density glass. While occurring sub-surface in the irradiation scheme shown, one might expect

Optical Materials EXPRESS

that this local volume change could be detectable in the near-surface region, were the irradiating intensity high enough to induce similar structure/morphology changes, albeit to a much lower extent.

To test this hypothesis, a two-dimension top-view Raman map of the modified glass ceramic's surface was generated and a corresponding refractive index map converted from the Raman map shows the spatially varying, localized structural changes near the laser-amorphized regions. Included for comparison are measurements made within a region above the written pillar as well as the un-irradiated region in the neighboring starting glass ceramic. Specifically, in calculating the Raman ratio of Ge-Se bond to As-Se bond peak intensities observed in such a map, we have previously shown the ability to correlate directly, such structural changes to a change in the local refractive index of the material [14]. Here, we use this established relationship to map and then predict the local refractive index of one of the irradiated lines over an area of 16 μm × 16 μm in the grating structure, and depict this index profile map in Fig. 4(b). As noted in Table 1, refractive indices (measured at λ = 4.5 μm) of starting glass ceramic and parent glass materials are 3.14 and 3.04, respectively. Examining the spatial dimensions of features observed in the map, the pillar diameter and the inter-pillar spacing are measured to be 4.8 μm and 9.2 μm which are very close to the targeted values of the beam waist, 4.43 μm, and pillar size, 9 μm, respectively. It is also important to note that the Raman beam spot size of 2 μm is smaller than the feature sizes (i.e., the pillar diameter and the inter-pillar spacing), making such spatial mapping of the laser-induced structure shown here, meaningful. The Raman ratio conversion to index (color scale of the legend is refractive index) used to predict the indices of the four pillars shows a post-exposure refractive index lower than that of the starting glass ceramic, closer to that of the base material. One can observe a gradual change in the region between pillars that shows an index increase closer to that of the pre-irradiated glass ceramic material. With the use of a flat-top laser beam and more overlap between the pillars, this graduation is expected to be reduced. To quantify the degree of LIV we can compare this spatial variation in the ratio of an index change between a region away from the irradiated region and a region in the center of a written pillar to that between a glass ceramic index and a glass index. The value is calculated to be 62%, indicating significant, partial re-vitrification. The magnitude of conversion from glass ceramic to glass is expected to be controllable via the choice of laser conditions [21]. The Raman signatures observed in the center of a written pillar, at the edge of a pillar, and away from the irradiated region [as indicated by the symbols C (black), E (red), and A (blue) in the index map] are shown in Fig. 4(c), and exhibit clear changes as a function of spatial position. A shift is observed from the center of the irradiated region towards the edge, which is likely due to decrease in the local irradiance from the Gaussian beam profile used. The Raman signal in the center of the pillar is nearly that of the base glass Raman signal shown in Figs. 3(c) and 4(a), confirming that the LIV has locally reorganized the partially crystallized glass ceramic's structure to be more glass-like. This is validated microscopically through electron microscopy evidence. Figure 4(d) shows a bright field (BF) TEM image and a corresponding SAED pattern of the laser-vitrified material. It is evident that the asymmetric crystals shown in Fig. 3(b) are converted to circular-shaped phases, and the number density of crystalline spots in the SAED pattern decreases upon laser irradiation. These circular features are likely partially crystallized and partially amorphous, possibly forming an intermediate step-wise progression back toward the phase separated (fully amorphous) morphology observed in the parent glass material [10]. The laser-modified microstructure is not entirely identical to the parent glass droplet/matrix morphology but similar enough to that shown in the dark field TEM image of a glass material (Fig. 3e top) and the corresponding SAED pattern (bottom) [10]. These features conclusively confirm that the proposed LIV process has occurred in these spatial regions. We foresee that further insight into the influence of the ultrashort pulse on the material's chemistry, phase transformation, and non-linear effects

Optical Materials EXPRESS

would be revealed by experiments such as lifetime measurements and time-resolved absorption.

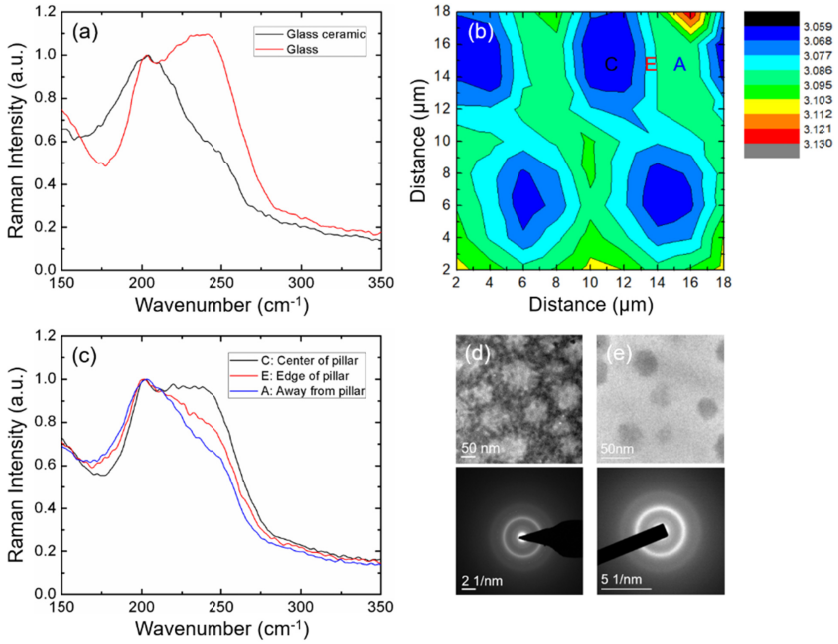

Fig. 4. (a) Raman spectra of starting glass ceramic and parent glass materials. (b) a Raman-converted refractive index profile map of a grating strip with four pillars that make up the strip. The legend indicates the refractive index scale corresponding to the colors shown. C (black), E (red) and A (blue) represent positions in the region directly above the center (C) of a pillar, at the edge of a pillar (E), and in an unirradiated region away (A) from a pillar (c) the corresponding Raman spectra collected at the center of a pillar (C), at the edge of the pillar (E), and away (A) from the pillar. Peak intensity has been normalized to 205 cm^{-1} (d) a BF TEM image and a corresponding SAED pattern of the laser-vitrified material. (e) a DF TEM image and a corresponding SAED pattern of the parent glass material.

Figure 5 shows the surface topography of the resulting laser-induced grating structure over an area of 1,600 μm × 1,600 μm as imaged using white light interferometry (WLI). The grating region was first characterized with WLI to determine if there was any laser irradiation-induced damage or local surface expansion. As it has been discussed previously that a local decrease crystallinity may result in a concurrent density reduction (increase in molar volume), it was surmised that expansion could likely take place in regions that had experienced re-amorphization. Expansion or contraction is commonly seen upon pulsed laser irradiation in many glass systems where laser irradiation leads to melting and rapid quenching inducing a local volume/density change [24]. To see this in the near-surface of the grating, two cut-through slices were taken from the surface WLI map/image. Shown in Fig. 5 and plotted as white lines on the figure (and depicted in the bottom traces for the respective slices), is the red line taken from a slice along the length of one irradiated line of pillars, where the blue line cuts orthogonally across all of the lines. As can be seen in the surface height modulation, these data confirm that surface expansion indeed exists in the irradiated regions. One can observe a very reproducible height change throughout all of the irradiated region, the magnitude which is surprising uniform considering the depth (mm's) below the surface where the modification is taking place. From the orthogonal line scan, one can see that the average inter-grating (period) spacing is measured to be 63 μm which is close to the targeted value of 60 μm. The average aspect ratio of the surface expansions is measured to be 2.4×10^{-3}, indicating a minimal, yet measurable volume expansion upon irradiation.

Optical Materials EXPRESS

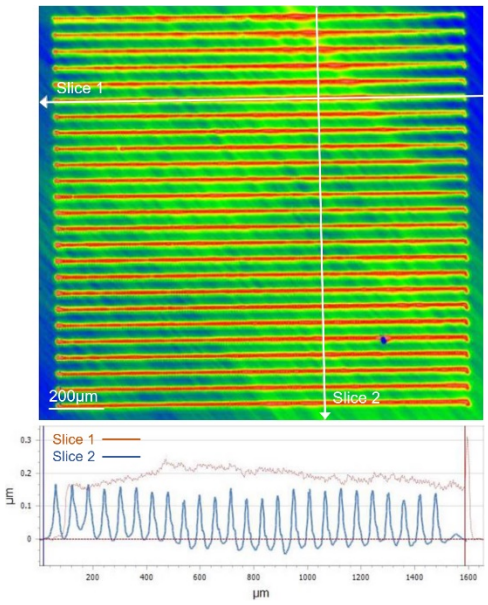

Fig. 5. (Top) A WLI image (area: 1,600 µm × 1,600 µm) of the laser- written grating surface illustrating the line patterns resulting from the pillar exposure modification to the bulk glass ceramic. (Bottom) Surface relief measured along a single laser written line (slice 1) and across all grating lines (slice two) within the laser-modified glass ceramic surface resulting in the LIV grating. Height profile variation are shown in microns.

To verify our proposed mechanism of laser-induced structural modification associated with the LIV process, microstructural characterization of the laser-induced grating was performed using TEM imaging. Here, analysis of a focused ion beam lift out-assisted cross-sectional specimen to identify the spatial variation of microstructures along the depth of the laser-irradiated region was carried out. Figure 6(a) shows a gradual morphological change from the glass ceramic surface into the material. BF TEM images with increased magnifications and their respective selective area electron diffraction (SAED) patterns are also shown on the right for the top, middle, and bottom regions of the specimen. Near the surface of the material, there are needle-like asymmetrical structures with fringes, indicating that the structures are crystalline. Deeper in the material, a phase-separated droplet-matrix morphology is seen as has been observed in the base glass of this material in our previous studies. A depth of an interface where the microstructure changes from needle-like crystals to droplets is measured to be ~3.5 µm below the surface. These micrographs definitely confirm that there is a gradient in the material from a more to less crystallized state as one migrates further into the material. The trend is supported by a decrease in the number and intensity of crystalline spots in the SAED patterns. As the focus of the laser was always inside of the material, the most intense irradiation would be observed further (deeper in 'z') into the bulk of the material. The existence of near-surface crystalline phases is consistent with the partial re-vitrification estimated by the index change ratio of 0.062. Furthermore, the depth-dependent microstructural transition from pristine, partially-crystalline glass ceramic to laser re-vitrified structures is consistent with the increasing values of laser power density as a function of depth extracted from Fig. 2(c) and overlaid on the large-area TEM image. A value of power laser density at the depth of the crystal-droplet microstructural transition (~3.5 µm) is attributed to a critical laser power density for an onset of re-vitrification process. In the present material system, this threshold for re-vitrification is estimated to be ~66.5 W/cm^2. Grazing-incidence μ-XRD was also performed on multiple locations in the laser-induced pattern and regions away from the patterned region to assess the spatial variation of crystallinity along the lateral distance upon irradiation, as shown in Figs. 6(b) and 6(c).

Optical Materials EXPRESS

Specifically, the spectra collected from the regions 1 - 7 in the inset of Fig. 6(b) clearly shows that the regions away from the pattern remain partially crystallized, as indicated by two peaks corresponding to crystalline As_2Se_3 and PbSe phases, while the crystallinity of the laser-irradiated region is significantly reduced, as indicated by the decrease or disappearance of the peaks [14,21]. To quantify the crystallinity of each region, the maximum intensity of the dominant peak located at $2\theta \approx 30°$ (associated with both PbSe and As_2Se_3 crystalline phases) is extracted from each spectrum, and is plotted in Fig. 6(c). The peak intensity, proportional to the crystallinity of the region of interest, substantially decreases in the laser-irradiated pattern, while the value increases in the region away from the pattern. These data further substantiate our explanation of the proposed LIV mechanism, and the bond-specific modification illustrated in the Raman ratio analysis.

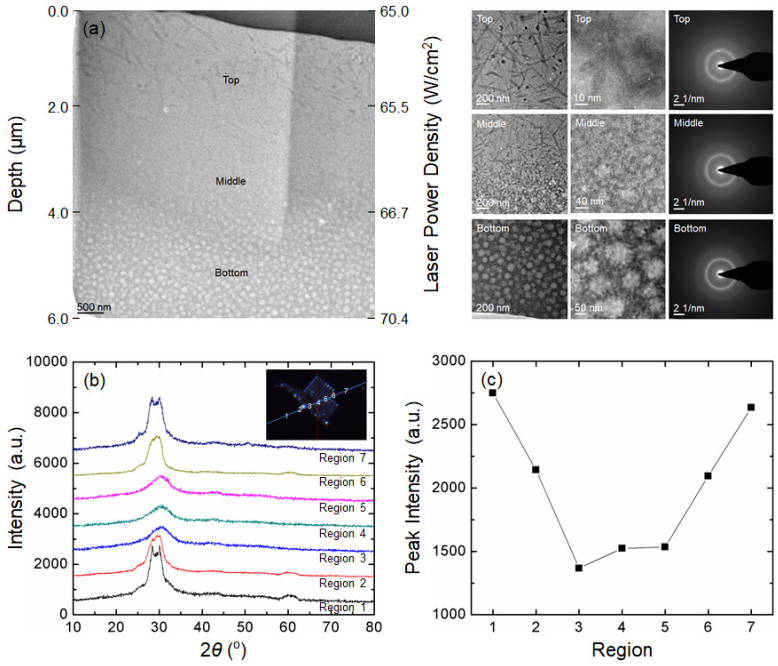

Fig. 6. (a) Bright field TEM images overlaid with a depth-dependent laser power density profile (left) and corresponding higher magnification TEM micrographs and SAED patterns for the top, middle, and bottom regions of the FIB-fabricated cross-sectional TEM specimen. (b) Grazing-incidence μ-XRD spectra collected from laser-induced grating regions and regions away from the structure. (c) A plot of integrated crystal phase peak intensity extracted from the XRD spectra for the positions identified in (b).

Lastly, to confirm the optical functionality of the LIV process, the written grating structure was evaluated by launching light into the diffractive structure and observing the diffracted beam orders. To assess the diffractive properties of the grating, the LIV structure was interrogated in both transmission (λ = 2 μm) and reflective (λ = 0.632 μm) modes. Under these measurement conditions, diffraction was confirmed by the presence of spots in the diffraction pattern as shown in Fig. 7. The spacing between the 0th-order (m = 0) and 1st-order (m = 1) spots in the reflection and transmission diffraction images correspond to reflection and transmission diffraction angles of 2.90° and 2.76°, respectively. Assuming a negligible impact of photo expansion with the surface expansion aspect ratio of 2.4×10^{-3}, an index difference between a region above a pillar and an inter-pillar region within the near-surface volume grating with a grating periodicity of 60 μm and a reflection and transmission diffraction angles of 2.90° and 2.76°, the calculated index change associated with the grating is estimated to be Δn ~-0.056 [21,25–27]. The index change closely matches that (–0.062)

Optical Materials EXPRESS

extracted from the Raman-converted index map in Fig. 4(b) with an error of 12.5%, confirming that LIV-induced local decrease in refractive index is evident. The refractive index drop is further supported by the fact that the reflection grating has multiple diffraction spots, while the transmission grating has less diffraction orders with less intensity in them since the decrease in the number and intensity of the diffracted orders is an indication of a local refractive index change in the material.

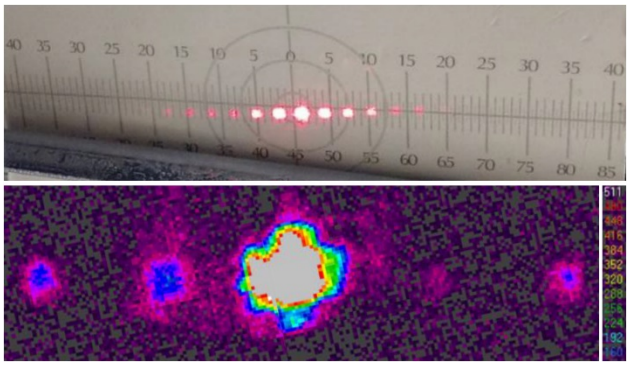

Fig. 7. Diffractive properties of the laser-written ChG grating measured in reflection at λ = 0.632 μm (top) and transmission at λ = 2 μm (bottom) for the LIV grating.

4. Conclusions

A novel laser-induced vitrification (LIV) technique based on absorption-induced heating was developed for a multi-component, GAP-Se chalcogenide material system which leads to spatially defined, re-amorphization of a glass ceramic material. The resulting multi-phase modification, which is adaptable to a range of glass/glass-ceramic materials, has been shown to result in optical functionalization of the post-processed material. The LIV technique has been shown to locally convert a partially crystallized glass ceramic into a composite containing discrete, laser-written glassy regions in the material as evidenced through a variety of characterization methods including Raman spectroscopy, XRD, and TEM. This work demonstrates a first-ever use of the LIV method to fabricate an index-graded structure, as shown in the production of an infrared volume grating. The LIV-written grating showed excellent uniformity with a grating period close to that designed by the laser-written pillar patterns. The extent of LIV (the magnitude of conversion from a glass ceramic to a glass) was determined to be 62% as quantified by use of a Raman mapping method which has been shown to correlate directly to refractive index modification. The LIV-written grating clearly shows depth-dependent microstructural transition from near-surface glass ceramic to fully re-vitrified structures, which has been shown to be consistent with the computed laser power density as a function of depth where a threshold power density for conversion has been quantified. The distance of the modification from the focal volume suggests that the irradiation threshold for phase conversion for this composition is near a laser power density level of 66.5 W/cm^2. Post-processed regions were shown to exhibit microscopic features suggestive of phase-separation similar to that observed in the parent glass prior to glass ceramic formation. Finally, employing the knowledge of laser-material modification and the correlation to phase conversion and index modification, the technique was successfully used to create and demonstrate for the first time, clear optical functionality in the form of an infrared diffraction grating.

Funding

This work was supported in part by the University of Central Florida. Laura Sisken acknowledges the Presidential Fellowship that assisted in supporting her graduate assistantship during this work.

Optical Materials EXPRESS

Acknowledgments

The authors acknowledge the helpful insight from discussions with Fedor Kompan, Ivan Divliansky, and Leonid B. Glebov.

References

1. B. J. Eggleton, B. Luther-Davies, and K. Richardson, "Chalcogenide photonics," Nat. Photonics **5**(3), 141–148 (2011).
2. R. Frerichs, "New optical glasses with good transparency in the infrared," J. Opt. Soc. Am. **43**(12), 1153 (1953).
3. S. Parvanov, V. Vassilev, and K. Tomova, "Optical properties of new chalcogenide glasses from the $GeSe_2$-Sb_2Se_3-PbSe system," Mater. Lett. **62**(12-13), 2021–2024 (2008).
4. J. S. Sanghera and I. D. Aggarwal, "Active and passive chalcogenide glass optical fibers for IR applications: a review," J. Non-Cryst. Solids **256-257**, 6–16 (1999).
5. S. D. Campbell, D. E. Brocker, J. Nagar, and D. H. Werner, "SWaP reduction regimes in achromatic GRIN singlets," Appl. Opt. **55**(13), 3594 (2016).
6. M. J. Booth, "Adaptive optical microscopy: the ongoing quest for a perfect image," Light Sci. Appl. **3**(4), e165 (2014).
7. D. T. Moore, "Gradient-index optics: a review," Appl. Opt. **19**(7), 1035–1038 (1980).
8. X. H. Zhang, H. Ma, and J. Lucas, "Evaluation of glass fibers from the Ga-Ge-Sb-Se system for infrared applications," Opt. Mater. **25**(1), 85–89 (2004).
9. X. H. Zhang, Y. Guimond, and Y. Bellec, "Production of complex chalcogenide glass optics by molding for thermal imaging," J. Non-Cryst. Solids **326-327**, 519–523 (2003).
10. A. Yadav, M. Kang, C. Smith, J. Lonergan, A. Buff, L. Sisken, K. Chamma, C. Blanco, J. Caraccio, T. Mayer, C. Rivero-Baleine, and K. Richardson, "Influence of phase separation on structure-property relationships in the $(GeSe_2\text{-}3As_2Se_3)_{1-x}PbSe_x$ glass system," Phys. Chem. Glasses **58**, 115 (2017).
11. L. Li, H. Lin, S. Qiao, Y. Zou, S. Danto, K. Richardson, J. D. Musgraves, N. Lu, and J. Hu, "Integrated flexible chalcogenide glass photonic devices," Nat. Photonics **8**(8), 643–649 (2014).
12. G. Yang, X. Zhang, J. Ren, Y. Yunxia, G. Chen, H. Ma, and J. L. Adam, "Glass formation and properties of chalcogenide in a $GeSe_2$-As_2Se_3-PbSe system," J. Am. Ceram. Soc. **90**(5), 1500–1503 (2007).
13. H. Wang, X. Zhang, G. Yang, Y. Xu, H. Ma, J. L. Adam, Z. Gu, and G. Chen, "Micro-crystallization of the infrared transmitting chalcogenide glass in $GeSe_2$-As_2Se_3-PbSe system," Ceram. Int. **35**(1), 83–86 (2009).
14. L. Sisken, C. Smith, A. Buff, M. Kang, K. Chamma, P. Wachtel, J. D. Musgraves, C. Rivero-Baleine, A. Kirk, M. Kalinowski, M. Melvin, T. S. Mayer, and K. Richardson, "Evidence of spatially selective refractive index modification in $15GeSe_2$-$45As_2Se_3$-40PbSe glass ceramic through correlation of structure and optical property measurements for GRIN applications," Opt. Mater. Express **7**(9), 3077 (2017).
15. F. Xia, X. Zhang, J. Ren, G. Chen, H. Ma, and J. L. Adam, "Glass formation and crystallization behavior of a novel GeS_2-Sb_2S_3-PbS chalcogenide glass system," J. Am. Ceram. Soc. **89**, 2154 (2006).
16. M. Kang, A. M. Swisher, A. V. Pogrebnyakov, L. Liu, A. Kirk, S. Aiken, L. Sisken, C. Lonergan, J. Cook, T. Malendevych, F. Kompan, I. Divliansky, L. B. Glebov, M. C. Richardson, C. Rivero-Baleine, C. G. Pantano, T. S. Mayer, and K. Richardson, "Ultra-low dispersion multicomponent thin film chalcogenide glass for broadband gradient index optics," in press, Adv. Mater. (2018).
17. A. Lepicard, F. Bondu, M. Kang, L. Sisken, A. Yadav, F. Adamietz, V. Rodriguez, K. Richardson, and M. Dussauze, "Long-lived monolithic micro-optics for multispectral GRIN applications," Sci. Rep. **8**(1), 7388 (2018).
18. P. R. Sahm, H. Jones, and C. M. Adam, *Science and Technology of the Undercooled Melt: Rapid Solidification Materials and Technologies* (Springer Netherlands, 2012).
19. B. Raj, *Frontiers in Materials Science* (Universities Press, 2005).
20. D. Lencer, M. Salinga, B. Grabowski, T. Hickel, J. Neugebauer, and M. Wuttig, "A map for phase-change materials," Nat. Mater. **7**(12), 972–977 (2008).
21. L. Sisken, "Laser-induced crystallization mechanisms in chalcogenide glass materials for advanced optical functionality," PhD Thesis, CREOL, College of Optics and Photonics, University of Central Florida (2017).
22. J. Chen and W. Z. Shen, "Raman study of phonon modes and disorder effects in $Pb_{1-x}Sr_xSe$ alloys grown by molecular beam epitaxy," J. Appl. Phys. **99**(1), 013513 (2006).
23. R. Zallen, M. L. Slade, and A. T. Ward, "Lattice Vibrations and Interlayer Interactions in Crystalline As_2S_3 and As_2Se_3," Phys. Rev. B **3**(12), 4257–4273 (1971).
24. J. W. Chan, T. Huser, J. S. Hayden, S. H. Risbud, and D. M. Krol, "Fluorescence spectroscopy of color centers generated in phosphate glasses after exposure to femtosecond laser pulses," J. Am. Ceram. Soc. **85**(5), 1037–1040 (2002).
25. R. Collier, C. B. Buckart, and L. H. Lin, *Optical Holography* (Academic, 1971).
26. D. J. Cooke and L. Solymar, "Comparison of two-wave geometrical optics and N-wave theories for volume phase holograms," J. Opt. Soc. Am. **70**, 1631 (1980).
27. A. Heifetz, J. T. Shen, and M. S. Shariar, "A simple method for Bragg diffraction in volume holographic gratings," Am. J. Phys. **77**(7), 623–628 (2009).